Promoting Hydrogen Production and Minimizing Catalyst Deactivation from the Steam Pyrolysis-Reforming of Biomass on nanosized NiZnAlOx Catalysts

Lisha Dong [a], Chunfei Wu [b*], Huajuan Ling[a], Jeffrey Shi[a], Paul T. Williams [c,*], Jun Huang [a,*]

[a] Laboratory for Catalysis Engineering, School of Chemical and Biomolecular Engineering, The University of Sydney, NSW 2006, Australia
(Tel: #61 2 9351 7483; Email: jun.huang@sydney.edu.au)
[b] School of Engineering, The University of Hull, Hull HU6 7RX, UK
(Tel: #44 1482 466464; Email: c.wu@hull.ac.uk)
[c] School of Chemical & Process Engineering, The University of Leeds, LS2 9JT, UK
(Tel: #44 1133432504; Email: p.t.williams@leeds.ac.uk)

Abstract: Hydrogen production from the thermochemical conversion of biomass was carried out with nano-sized NiZnAlOx catalysts using a two-stage fixed bed reaction system. The vapors derived from the pyrolysis of wood sawdust were catalytically steam reformed in the second reactor. The NiZnAlOx catalysts were synthesized by co-precipitation method with different Ni molar fractions (5, 10, 15, 25 and 35%) and a constant Zn:Al molar ratio of 1:4. The catalysts were characterized by a wide range of techniques, including N_2 adsorption, SEM, XRD, TEM and temperature-programmed oxidation (TPO) and reduction (TPR). Fine metal particles of size around 10-11 nm were obtained and the catalysts had high stability characteristics for all the fresh catalysts, which improved the dispersion of active centers during the reaction and promoted the performance of catalysts. The yield of gas was increased from 49.3 to 74.8 wt.%, and the volumetric concentration of hydrogen was increased from 34.7 to 48.1 vol.%, when the amount of Ni loading was increased from 5 to 35%. Meanwhile, the CH_4 fraction decreased from 10.2 to 0.2 vol.% and the C_2-C_4 fraction was reduced from 2.4 vol.% to 0.0 vol.%. During the reaction, the crystal size of all catalysts was successfully maintained at around 10-11 nm with negligible coke formation, and no obvious sintering detected. The efficient production of hydrogen from the thermochemical conversion of renewable biomass indicates that it is a promising sustainable method to generate hydrogen from biomass with the NiZnAl metal oxide catalyst prepared in this work via a two-stage reaction system.

Key Words: Biomass; Catalyst; Hydrogen; Coke; Sintering

1. Introduction

There are key environmental challenges for the use of fossil fuels in relation to energy security, environmental impact and the release of greenhouse gases. There is global interest in the development of renewable and clean fuels as alternatives to fossil fuels [1-4]. Hydrogen is known as an ideal clean energy carrier for the production of heat and power, since its combustion releases only water [4, 5]. The utilization of hydrogen for electricity generation via fuel cells and power plant has been recognized, with high efficiencies and zero net contribution of CO_2 to the atmosphere [6]. Efforts are developing towards cost-efficient processes to produce sufficient hydrogen from renewable resources e.g. wind, hydropower, and biomass for commercial utilization [7-10]. Among these resources, biomass is abundantly available including cheap and non-food feedstocks, such as energy crops, agricultural residues, organic wastes, by-products from bio-refineries and wastes produced by the food industry, and the biodegradable fraction of municipal solid waste [11, 12]. From a technical point of view, sustainable hydrogen produced from biomass by thermochemical processes e.g. gasification and pyrolysis has already been developed [13, 14, 15].

Therefore, biomass gasification for hydrogen production has drawn great interest, particularly using steam as the gasification agent and a suitable catalyst where the hydrogen yield can be significantly enhanced [16-20]. However, a challenge towards large scale commercialisation is tar formation in the product syngas and coke formation on the catalyst; the tar can block the pipework of downstream applications and the coke deposits on the surface of the reacted catalyst lead to deactivation [21]. A desirable catalyst should promote tar reduction in the syngas, have good thermal stability in terms of prohibition of metal sintering and promote a high yield of hydrogen production. [21-23] A number of catalysts have been proven to be active for hydrogen production and are stable towards deactivation in biomass gasification, which are mainly the platinum group metal (e.g. Ph, Rt, Pd, Ru) based catalysts[23-27]. However, the high cost of noble metal-based catalysts discourages the practical application of biomass gasification. Therefore, to develop a cheaper and alternative metal-based catalyst would be desirable [4].

During the last decade, nickel-catalysts have been extensively investigated for biomass gasification. For enhanced catalytic performance and thermal stability, various supports (such as, zeolites [4, 5, 7, 28, 29], dolomite [1, 22, 30, 31], olivine [21, 32], other metal and metal oxides

such as La, Fe, CeO_2, SiO_2, ZrO_2, TiO_2, MgO, ZnO, Al_2O_3 [10, 33-39]) have been applied to change the interactions between support and metal particles which may thereby influence the catalytic properties. Particularly, alumina has been widely investigated as a catalyst support due to high activity and low cost in the reforming process [33-35, 40]. However, catalysts based on an alumina support suffer severely from coke deposition because of the strong acidity of the alumina support [41]. Under this circumstance, modifications of Ni-based Al_2O_3 supported catalysts should be investigated by the addition of basic metals or promoters which can help decrease the support acidity and also improve the prohibition of coke formation on the surface of the catalyst and also the catalyst thermal stability [21].

The application of basic metal oxides [42, 43] as supports or as promoters [44, 45] into Al_2O_3 have been researched to enhance the catalytic performance and minimize the coke deposition. For example, Yang et al. [46] investigated the effect of catalyst supports on ethanol steam reforming (ESR) using Ni-based catalysts and reported that Ni/ZnO exhibited the highest hydrogen selectivity followed by Ni/MgO and Ni/Y-Al_2O_3. Ethanol steam reforming using ZnO/Al_2O_3 was carried out by Chen et al. [47], and it was found that the introduction of ZnO is beneficial to the reduction of CO production, avoiding the initial loss of catalytic activity and thus enhancing the long-term catalyst stability. Monzón et al. [48] also reported that the introduction of ZnO in Ni/Al_2O_3 increased the H_2 selectivity with reduced coke deposition. Abello et al. [3, 49] studied ethanol steam reforming with a Ni/Zn–Al catalyst prepared by a sol-gel method and found that the catalyst had high selectivity to H_2 and CO_2. In the methanol steam reforming reported by Yang et al. [50], ZnO-Al_2O_3 exhibited high hydrogen yield with low CO concentration. Therefore, the addition of basic ZnO into Ni-based Al_2O_3 catalysts could be promising for the process of steam gasification of biomass.

Biomass gasification has been investigated with single [21] or two-stage reaction systems [1, 4, 5, 7, 51]. Under the single stage reaction systems, the samples and catalysts were mixed and the pyrolysis and gasification processes were operated under the same conditions, resulting in difficulty in the separation of catalysts and biomass residues after reaction [21]. A two-stage pyrolysis-catalytic reforming system can overcome this challenge and improve gas quality since the thermal degradation of the biomass and reforming of derived products are under different process conditions e.g. temperature.

In this work, co-precipitated NiO-ZnO-Al_2O_3 catalysts were prepared and used for the

catalytic steam reforming of the derived volatile products from the pyrolysis of wood sawdust, by using a fixed bed, two-stage reaction system. The aim was to enhance hydrogen production but minimize coke deposition on the reacted catalyst whilst maintaining catalyst stability.

2. Experimental

2.1. Preparation of materials and fresh catalysts

The properties of the raw materials (wood sawdust) utilized was presented in our previous report [7]. The proximate analysis of the wood sawdust was 5.7 wt.% moisture, 74.8 wt.% volatiles, 18.3 wt.% fixed carbon, and 1.2 wt.% ash. The ultimate analysis showed that the wood sawdust was 5.9 wt.% hydrogen, 47.1 wt.% carbon, 0.1 wt.% nitrogen and 46.9 wt.% oxygen which was obtained by mass difference.

The NiO-ZnO-Al_2O_3 catalysts with different Ni molar ratios (5, 10, 15, 25, and 35%) and a constant Zn:Al molar ratio (Zn:Al=1:4) were obtained by co-precipitation method [10, 52, 53]. $Ni(NO_3)_2 \cdot 6H_2O$, $Zn(NO_3)_2 \cdot 6H_2O$, $Al(NO_3)_3 \cdot 9H_2O$ (Sigma-Aldrich, Australia) were dissolved in deionized water to form a 1 mol L^{-1} solution. The mixture of nitrated solutions with Zn:Al molar ratio of 1:4 was precipitated using with 2 mol L^{-1} $NH_3 \cdot H_2O$ (Sigma-Aldrich, Australia) solution, adding drop by drop. When the pH of the suspension was around 8, the addition of ammonia solution was stopped. The suspension was then aged under agitation for one hour at 60 °C and filtered under vacuum. The obtained filter cake was dried in oven at 80 °C for about 8 h. Finally, the precursor was calcined under air atmosphere at 800 °C for 4 hours with a heating rate of 1 °C min^{-1}. The calcined fresh catalyst was ground into fine powders and sieved to obtain particle sizes with a range between 50 and 180 μm. The fresh NiZnAl catalysts were denoted as xNiZnAl where "x" indicates the nickel molar ratio (%), e.g. 5, 10, 15, 25 and 35.

2.2. Pyrolysis catalytic reforming of biomass

The prepared NiO-ZnO-Al_2O_3 catalysts were tested for hydrogen production from thermochemical conversion of biomass. A two-stage reactor was used in this work. In the first reactor, the wood sawdust was decomposed into pyrolysis vapors, which passed to the second reactor for catalytic steam reforming reactions for the production of hydrogen. The schematic

diagram of the two-stage fixed bed reaction system was presented in our previous report [4].

For each experiment, N_2 was used as carrier gas with a flow rate of 80 ml min^{-1}. 0.8 g wood sawdust and 0.25 g fresh NiO-ZnO-Al_2O_3 catalyst were placed in the first and second reactor, respectively. The temperature of the catalyst reactor was initially heated to 800 °C [54]. When the second reactor (catalyst bed) was stabilized at 800 °C, the first reactor where the biomass sample was placed was heated to 535 °C at 40 °C min^{-1}. Steam was generated by heating water, which was injected to the second reactor with a flow rate of 4.74 ml h^{-1} using a syringe pump when the pyrolysis reactor was started to be heated. In this work, sand was used instead of the catalyst for the blank experiment.

The liquid product derived from the catalyst bed was collected with two condensers, which were air cooled and dry-ice cooled, respectively. A 25L Tedlar^{TM} gas bag was used to collect the non-condensed gases, which were further analyzed using off-line gas chromatograph (GC). The gas, residue yields and mass balance was calculated via the following Equations (1), (2) and (3), respectively:

$$\text{Gas Yield (wt.\%)} = \frac{\text{Gas mass}}{\text{Wood sawdust mass}} \times 100 \qquad \text{Equation (1)}$$

$$\text{Residue Yield (wt.\%)} = \frac{\text{Residue mass}}{\text{Wood sawdust mass}} \times 100 \qquad \text{Equation (2)}$$

$$\text{Mass balance (wt.\%)} = \frac{\text{Gas mass + Residue mass + Liquid mass + Char mass}}{\text{Wood sawdust mass + injected water mass}} \times 100 \qquad \text{Equation (3)}$$

It is noted that the mass of reside after pyrolysis was obtained by the mass difference of the sample boat before and after the experiment. The total reaction time for each experiment was about 40 min. Each catalyst was used once for the experiment. In addition, the experiment with a mass balance close to 100% was used for analysis. Selected experiments were repeated, for example, the standard deviations using the 35NiZnAl catalysts are: 0.69 for hydrogen yield, 2.27 for hydrogen concentration, 1.81 for CO_2 concentration and 0.18 for CH_4 concentration.

2.3. Characterizations of gas

C_1 to C_4 hydrocarbons were analyzed with a Varian 3380 GC with a flame ionization detector (FID). An HayeSep column (80-100 mesh) and carrier gas (N_2) were used. H_2, CO and N_2 were determined using a Varian 3380 GC with a molecular sieve column (60-80 mesh) and

argon was the carrier gas. CO_2 gas was analyzed by another Varian 3380 GC on a HayeSep column (80-100 mesh) with carrier gas (argon).

2.4. Analysis of catalysts

N_2 adsorption isotherms (Quantachrome Autosorb-1) were used to obtain the specific surface area of the fresh NiO-ZnO-Al_2O_3 catalyst. Prior to the isotherm analysis, about 150 mg of catalyst was degassed under vacuum for 5h at 150 °C. The 5-point Brunauer, Emmett and Teller (BET) method was used to evaluate the surface area of the fresh catalyst.

X-ray diffraction (XRD) patterns of the fresh catalysts were determined using a SIEMENS D5000 instrument using Cu Kα radiation. The scanning range was between 10 and 70° and the scanning step was 0.02°. The crystal particle size (D) of the catalyst was obtained using Scherrer's formula.

The morphologies of the catalysts were analyzed by a scanning electron microscope (SEM) (LEO 1530). In addition, transmission Electron microscopy (TEM) (Phillips CM120 BioFilter) analysis was carried out to obtain detailed information about the fresh NiO-ZnO-Al_2O_3 catalysts The reducibility of the prepared fresh catalysts was analyzed by temperature programmed reduction (TPR) using a thermogravimetric analyzer (SDT Q600). During the TPR analysis, about 15 mg fresh NiO-ZnO-Al_2O_3 catalyst was used. The catalyst sample was heated from room temperature to about 1200 °C at 10 °C min^{-1} using 15 vol.% H_2 gas balanced with 85 vol.% N_2 (total flow rate was 100 mL min^{-1}).

3. Results and Discussion

3.1. Characterizations of the fresh NiZnAl catalysts

3.1.1. N_2 adsorption and XRD analysis of fresh NiO-ZnO-Al_2O_3 catalysts

Textural properties, theoretical metal composition and BET surface area are shown in Table 1. The specific surface area of the fresh catalysts were 83.2 - 95.7 m^2 g^{-1}. It seems that increasing the Ni molar ratio from 5 to 35% did not significantly change the surface areas of catalysts. XRD patterns of the fresh NiO-ZnO-Al_2O_3 catalysts are shown in Fig. 1, and the particle size of crystals

in the NiO-ZnO-Al_2O_3 calculated from the XRD analysis are summarized in Table 1. It has been found that $ZnAl_2O_4$ spinel structure was easily formed compared to $NiAl_2O_4$ spinel when the ions of Zn^{2+}, Al^{3+} and Ni^{2+} coexisted inside the NiO-ZnO-Al_2O_3 catalyst, because Zn^{2+} ions can easily enter into the tetrahedral sites of the interstices between O^{2-} ions while Ni^{2+} ions are difficult to enter into the close-packed O^{2-} ionic lattice [55]. From the XRD results, the presence of spinel $ZnAl_2O_4$ phase (JCPDS 05-0669), characterized by two intense and symmetric peaks at 2θ=31.3° and 36.9° and other less intense peaks at higher 2θ values (2θ=59.4°, 65.3°), was clearly evidenced in all the fresh NiO-ZnO-Al_2O_3 catalysts, which is consistent with the results reported by Barroso et al. [3]. Meanwhile, the peak at 2θ=65.3° for stoichiometric $NiAl_2O_4$ spinel was displayed in all XRD patterns of fresh catalysts, the other peaks for the $NiAl_2O_4$ spinel phase which occur at values of approximately 2θ=19.1°, 31.4°, 37.0°, 45.0°, 55.9°, 59.6° also appeared distinctly (JCPDS 78-0552) [56]. A small crystal size (6-7 nm) of the spinel was calculated based on the Scherrer equation (Eq.(4)).

$$\tau = \frac{K\lambda}{\beta \cos\theta} \qquad \text{Equation (4)}$$

where τ is the mean size of crystal particles; K is dimensionless shape factor; λ is the X-ray wavelength; β is the line broadening at half the maximum intensity; and β is the Bragg angle.

Based on the study of Buitrago-Sierra et al. [41], the most intense diffraction peak of ZnO at around 36.8° overlaps over the most intense $ZnAl_2O_4$ diffraction peak. A diffraction peak at 34.8° is assigned to discrete ZnO. However, in this work, no evidence shows the presence of ZnO in the fresh NiO-ZnO-Al_2O_3 catalysts. This effect may be due to the fact that ZnO has completely reacted with Al_2O_3 upon calcination to form the $ZnAl_2O_4$ spinel phase. Meanwhile, the presence of Al_2O_3 was not obtained, which may be that the amount of remaining Al_2O_3 was too small to be detected [41] or due to the fact that γ-Al_2O_3 has poor crystallinity [3]. Furthermore, according to Buitrago-Sierra et al. [57], XRD typically detects crystallites that are larger than 2-5 nm; thus, it is possible that ZnO, NiO and Al_2O_3 exist on these catalysts have crystallite size smaller than the detection limit [56].

With increasing the Ni molar ratio to 15%, the appearance of NiO was still not identified, which may due to more $NiAl_2O_4$ spinel formation or the size/amount of remaining NiO was too small to be detected by XRD [41]. Further increasing the Ni molar ratio to 25, and 35%, the diffraction peaks for NiO at values of approximately 2θ=43.3° and 62.9° (JDPDS 89-7131) were clearly evidenced and the main peak for NiO at the value of 2θ=37.0° may overlap with the peak

of $NiAl_2O_4$ (JCPDS 78-1601) at the similar position of 2θ values [41, 56, 58].

$ZnAl_2O_4$, $NiAl_2O_4$ phases with a crystallite size of approximate 6-7 nm, which were calculated based on the Scherrer equation, were assigned in the XRD patterns for all fresh NiO-ZnO-Al_2O_3 catalysts. In addition, NiO phases with a particle size of approximate 7 nm were identified in the XRD patterns for fresh NiO-ZnO-Al_2O_3 catalysts with a Ni molar ratio of 25 and 35%. The $ZnAl_2O_4$, $NiAl_2O_4$ and NiO particle sizes were calculated based on $ZnAl_2O_4$, $NiAl_2O_4$ and NiO diffraction peaks at the same 2θ value of 37.0º in the XRD patterns for all fresh NiO-ZnO-Al_2O_3 catalysts.

3.1.2. SEM and TEM analysis of the fresh NiZnAl

SEM images of the fresh NiO-ZnO-Al_2O_3 catalysts are shown in Fig. 2 to characterize the morphology of the catalysts. Increasing the Ni molar ratio from 5 to 15%, produced very similar morphologies (Fig. 2 (a), (b) and (c)). The micrographs which can be seen from Fig. 1(a), (b), and (c) show the presence of agglomerates composed of small quasi-spherical particles in the micrometric scale. Further increasing Ni molar ratio to 25 and 35%, resulted in more metal oxide particles being dispersed on the surface until clusters are formed (Fig. 2(d) and Fig. 2(e)). From Fig. 2(d) and Fig. 2(e), the metal oxide clusters are densely dispersed on the surface, and it is difficult to differentiate $ZnAl_2O_4$, $NiAl_2O_4$ and NiO particles which have been identified from XRD (Fig. 1).

The TEM images of the fresh 5NiZnAl and 35NiZnAl catalysts in scales of 20 and 50 nm are depicted in Fig. 3. From Fig.3, a high dispersion of the metal oxide particles can be observed. The particle size obtained from TEM images was around 6-7 nm which is consistent with the XRD results as shown in Table 1 for the 5NiZnAl and the 35NiZnAl catalysts. From the XRD, SEM and TEM analysis of the fresh catalysts, it is suggested that nano-metal particles are successfully dispersed on the surface of the NiO-ZnO-Al_2O_3 catalysts, indicating a high dispersion of metal particles was obtained.

3.1.3. TPR analysis of fresh NiZnAl catalysts

The TPR analysis of the fresh catalyst was performed to study the reduction properties of surface metal oxide compounds on fresh catalysts. As shown in Fig. 4, for the fresh 5NiZnAl and 10NiZnAl catalysts, a broad hydrogen consumption band is obtained between 650 and 1050 °C

with a maximum consumption at around 1000 °C, and these can be assigned to the reductions of $ZnAl_2O_4$ and $NiAl_2O_4$ spinel phases [59-61]. High temperature was required to reduce the fresh catalyst; it is suggested that this was due to the strong interactions between metals and catalyst support [56].

When the Ni molar ratio was increased to 15%, an extra reduction peak was observed at around 830 °C, in relation to the reduction of stoichiometric $NiAl_2O_4$ spinel phase [56, 62]. When the Ni molar ratio was further increased to 25, and 35%, a reduction peak at around 500 °C can be related to the reduction of NiO [56]. Ni content has been reported to dissolve preferably with Al_2O_3 support at high temperature to form $NiAl_2O_4$ spinel phase when Ni loading was low; with the increase of Ni content, bulk NiO particles were formed [58, 62].

It is noted that for all the fresh catalysts, the reduction of $ZnAl_2O_4$ or $NiAl_2O_4$ migrated from around 1000 to 900 °C with increasing Ni content. This result is consistent with the literature investigating catalysts prepared by sol-gel and co-precipitation [60, 61, 63, 64]. For example, Guo et al. [63] investigated nickel catalysts with $MgAl_2O_4$ spinel as support using TPR analysis and two reduction peaks were found; the maximum reduction temperature of the second peak was moved from 800 to 705 °C with the increase of Ni loading from 1 to 15 wt.%.

3.2. Wood sawdust pyrolysis and catalytic reforming with NiO-ZnO-Al_2O_3 catalysts

3.2.1. Product yield

Gas and hydrogen production of the pyrolysis-catalytic steam reforming of wood sawdust is shown in Table 2. The residue yield stabilized at around 37.5 wt.% in this work since pyrolysis in the first stage reactor was the same for each experiment. Liquid products collected from the condensers consisted of a mixture of bio-oil and non-reacted water. The mass of the injected water into the reaction system was calculated by the weight difference of the syringe.

For the blank experiment using a sand bed, the gas yield in relation to the mass of wood sawdust was 33.0 wt.%, and the hydrogen production was 2.4 mmol H_2 g^{-1} wood sawdust (Table 2). However, with the addition of NiO-ZnO-Al_2O_3 catalysts with Ni molar ratios ranging from 5 to 35%, both the gas and hydrogen yields were enhanced gradually and significantly, from 49.3 to 74.8 wt.% and from 8.2 to 20.1 mmol H_2 g^{-1} wood sawdust, respectively. It indicates that the NiO-

$ZnO\text{-}Al_2O_3$ catalyst is efficient for hydrogen production from pyrolysis catalytic reforming of wood sawdust.

$ZnAl_2O_4$ phases were reported to increase the production of hydrogen by the promotion of water gas shift reaction, when steam reforming of ethanol was investigated using Ni/Al_2O_3 catalysts promoted by Zn [41]. The influence of Ni content on hydrogen production has been reported by other researchers. For example, Corujo et al. [31] investigated the catalytic activity of a Ni/Dolomite catalyst for the gasification of forestry residue in the presence of steam. They reported that the optimal result in terms of hydrogen production was found with the catalyst loaded containing the smallest amount of NiO (0.4Ni/Dolomite). NiZnAl catalysts with different atomic ratios of Zn/Al (0-25 wt.% Ni amount) were used for ethanol steam reforming; high hydrogen production and selectivity were observed on the catalysts containing nickel amount between 18 and 25 wt.% [3]. In our previous work [7], the pyrolysis and steam reforming of wood sawdust with a Ni/MCM-41 catalyst was studied. When the Ni content in the Ni/MCM-41 catalyst was increased from 5 to 40 wt.%, the gas production was increased from 40.7 to 62.8 wt.% and the H_2 yield was enhanced from 6.2 to 18.2 mmol H_2 g^{-1} sample, respectively.

Smaller metal particle size and more catalytic active sites were reported to enhance gas production from reforming reactions [3, 59, 65]. For example, during biomass gasification with Ni/MCM-41 catalyst [7], the production of hydrogen and gas was significantly increased with the increase of Ni loading from 5 to 20 wt.% while NiO crystal size was stable (around 2.9 nm). However, with the further increase of Ni loading to 40 wt.%, gas and hydrogen showed slight changes; this was suggested to be due to the enlargement of NiO particles. In addition, $ZnAl_2O_4$ supported Pt catalysts applied in the n-butane dehydrogenation process was investigated [65]. The Pt catalysts with $ZnAl_2O_4$ prepared by co-precipitation method presented high catalytic activity and product selectivity compared to the $ZnAl_2O_4$ catalysts prepared by mechanochemical synthesis. This was due to the $ZnAl_2O_4$ catalyst being prepared by co-precipitation method which had higher dispersion of metal particles.

In this work, the average size of metal particles is about 6 nm, calculated from the XRD analysis (Table 1 and Fig.1). In addition, the metal particle size was maintained when the Ni content was increased from 5 to 35%. Therefore, higher yields of gas and hydrogen were obtained with the increase of catalytic sites during pyrolysis-catalytic reforming of wood sawdust in this work. Furthermore, TPR analysis also suggests that more catalytic sites were generated with the

increase of Ni content from 5 to 35% as the catalyst becomes more reducible (Fig.4).

3.2.2. Gas concentration

In this work, the biomass was initially pyrolysed to produce H_2O, H_2, CO, CO_2, CH_4， tar, char and organic volatiles (Eq. (5)) in the first stage pyrolysis reactor, followed by the reforming of tar and organic volatiles in the second stage. The second stage includes reactions of CO, CO_2, H_2 and H_2O with the hydrocarbons and oxygenated compounds derived from pyrolysis of wood sawdust, thereby producing gaseous products. It is noted that the concentration of carrier gas (N_2) was around 90 vol.% for each catalytic experiment. In this work, N_2 free concentrations were used for the produced gases e.g. CO and H_2 in Table 2.

The steam atmosphere and the utilization of catalyst promote the decomposition and reforming reactions so that more light gases, such as H_2, CO, CH_4 and CO_2 are produced [66]. It is well known that water-gas shift reaction (Eq.(6)), steam reforming of hydrocarbons and oxygenated compounds (Eq. (7) and Eq. (8)), CO_2 reforming of hydrocarbons and oxygenated compounds (Eq. (9) and Eq. (10)), decomposition reactions of hydrocarbons and oxygenated compounds, carbon gasification reaction (Eq. (13)) together with Boudouard reaction (Eq. (14)) were the main reactions which occurred parallel and contributed to the high gas and H_2 yields [67].

$$Biomass \rightarrow H_2O + H_2 + CO + CO_2 + tar + char + volatiles \quad \text{Equation 5}$$

$$CO + H_2O \leftrightarrow CO_2 + H_2 \quad \text{Equation 6}$$

$$C_mH_n + H_2O \rightarrow CO + H_2 \quad \text{Equation 7}$$

$$C_xH_yO_z + H_2O \rightarrow CO + H_2 \quad \text{Equation 8}$$

$$C_mH_n + CO_2 \rightarrow CO + H_2 \quad \text{Equation 9}$$

$$C_xH_yO_z + CO_2 \rightarrow CO + H_2 \quad \text{Equation 10}$$

$$C + H_2O \rightarrow CO + CO_2 + H_2 \quad \text{Equation 11}$$

$$C + CO_2 \rightarrow 2CO \quad \text{Equation 12}$$

$$CO_2 + CH_4 \rightarrow CO + H_2 \quad \text{Equation 13}$$

Gas composition for the non-condensed gas product after the steam reforming of derived products from pyrolysis of wood sawdust are listed in Table 2. CO, H_2, CO_2 and CH_4 were found

to be the main gases from the non-catalytic steam reforming process with a sand bed (45.5 vol.% of CO, 17.4 vol.% of H_2, 14.5 vol.% of CO_2 and 14.8 vol.% of CH_4). Increasing the Ni content to 10%, the gas concentration showed a similar but not significant trend as increasing the Ni molar ratio from 0 to 5%. The CO, CH_4 and C_2-C_4 concentrations slightly decreased from 33.8 to 32.7 vol.%, from 10.2 to 8.9 vol.% and from 2.4 to 1.3 vol.%, respectively. While the H_2 content increased from 34.7 to 38.1 vol.% with the similar amount of CO_2 (from 18.9 to 19.0 vol.%). Both water gas shift reaction and dry reforming contributed to the process. Further increasing the Ni molar ratio to 15%, the H_2 concentration increased continuously from 32.7 to 37.3 vol.% and the CH_4 content was diminished from 8.9 to 6.3 vol.%. However, the CO concentration increased from 32.7 to 37.3 vol.%, CO_2 content was consumed from 19.0 to 16.2 vol.% with the similar C_2-C_4 concentration (from 1.3 to 1.5 vol.%), which might be attributed to the CO_2 dry reforming with methane (Eq.(13)). With the increase of the Ni molar ratio continuously from 15% to 25%, the H_2 content increased significantly from 38.7 to 46.9 vol.%, CH_4 and C_2-C_4 concentration were decreased from 6.3 to 0.9 vol.% and from 1.5 to 0.2 vol.%, respectively, with the similar reductions for CO (from 37.3 to 36.7vol.%) and CO_2 amount (from 16.2 to 15.3 vol.%). Obviously, steam reforming of hydrocarbons mainly contributed to the process. The produced CO should be consumed by the water-gas shift reaction (Eq.(6)). The amount of CO_2 would be balanced after dry reforming of hydrocarbons, which has been promoted by the increased Ni catalytic active sites.

According to the GC/MS analysis results of the liquid product as shown in Table 3, major chemical compounds appeared in the bio-oil collected in the steam reforming reactions carried out with sand and catalysts with a lower Ni content, such as phenol (methyl-), naphthalene (methyl-), acenaphthylene, and fluorene, while the peaks assigned to those compounds disappeared when the Ni molar ratio reached 25%. It was confirmed again that high Ni loading would promote hydrocarbon reforming.

When the Ni molar ratio was increased to 35%, the H_2 concentration was enhanced continuously from 46.9 to 48.1 vol.%, the CO content in total gas was kept constant around 36.7 vol.%, and CO_2, CH_4 and C_2-C_4 concentration were all slightly decreased, from 15.3 to 15.1 vol.%, from 0.9 to 0.2 vol.% and from 0.2 to <0.1 vol.%, respectively, which indicates that the major reactions which occurred were CO_2 reforming and decomposition reactions of hydrocarbons and oxygenated compounds via Eq. (7)-(10). This was also supported by GC/MS results for the liquid product shown in Table 3, showing heavy molecular weight chemical compounds in the bio-oil

were not detected with the catalysts with the highest Ni loading. Similar changes of the gas composition were reported based on the work of Barroso et al. [3] that the H_2 concentration increased while the CH_4 and C_2-C_4 concentrations decreased with the increase of Ni content during the ethanol steam reforming on a NiZnAl catalyst prepared by incipient wet impregnation method.

According to the gas composition data in Table 2, the highest gas and H_2 yields were obtained from the steam reforming process carried out with the 35NiZn4Al catalyst, the highest H_2/CO ratio was obtained with 25NiZn4Al and 35NiZn4Al catalysts, while the lowest the CO/CO_2 ratio was obtained with the utilization of 10NiZn4Al catalyst.

The gas composition performance of biomass catalytic steam gasification has also been studied by other researchers [1, 7, 31, 40, 66]. Among the aforementioned reports for investigating the influence of Ni loading on gas concentrations during steam reforming of hydrocarbon, it was found that H_2 was increased and concentrations of CH_4 and C_2-C_4 were reduced. However, changes of CO and CO_2 concentrations could be different since CO and CO_2 were produced and consumed in parallel based on Eq. (7)-(11). For example, Corujo et al. [31] reported that CO concentration was increased and CO_2 concentration was decreased with the increase of Ni loading from 0.4 to 4.3 wt.% of Ni/Dolomite catalysts during the steam gasification of forestry residue. While different trends for CO and CO_2 gases were found in the steam gasification of biomass in the presence of Ni/MCM-41 catalysts with a Ni loading ranging from 5 to 40 wt.% [7], which is consistent with the promotion of the water-gas shift reaction (Eq. (6)).

3.3. Investigation of coke deposition on the reacted catalysts

TPO analysis was carried out to the reacted catalysts and the results are depicted in Figure 6 via weight change versus temperature. Two oxidation stages in the TPO analysis are shown in Figure 6, metal particle oxidation and carbon oxidation. The peaks of increasing mass from 250 to 500 °C and above 700 °C were assigned to the oxidation of Ni, Zn and other reduced metal species during the TPO analysis. The reduced metal species are suggested to be produced during the pyrolysis and gasification process where the reduction agents, H_2 and CO, were present and therefore the fresh catalysts did not need to be reduced before gasification experiments [7].

The weight loss before 550 °C for the TPO analysis might be assigned to the oxidation of amorphous carbons. The oxidation peak at a higher temperature which starts from 550 to 700 °C

might be attributed to the oxidation of carbon deposited on the catalyst surface, probably filamentous carbon [68, 69]. The amount of the coke formation was obtained from the weight loss of catalyst during the TPO analysis divided by the initial sample weight. It is noted that the weight increase in Figure 6 was ascribed to the oxidation of metallic sites (Ni), which was produced during the reactions. In this work, the weight increased was not considered for the calculation of coke formation. It is demonstrated from Figure 6 that the total amount of coke deposition was 0.1 wt.% of the used NiO-ZnO-Al_2O_3 catalyst with a Ni molar ratio of 35%, which can be considered as negligible indicating that coke resistant catalysts have been obtained after adding Zn during the synthesis in this work. Corujo et al. [31] reported more than 5 wt.% amount of coke formation on a Ni/dolomite catalyst for the steam gasification of forestry residue and an even higher amount (>10wt.%) of coke formation was obtained on a reacted Ni/Al_2O_3 catalyst for the steam gasification of biomass reported by Nishikawa et al. [24].

The presence of amorphous and filamentous carbons ("whiskers") on the surface of the reacted catalysts was also confirmed by SEM analysis, shown in Figure 7. However, due to the low amount of carbon deposition, the appearance of filamentous carbon does not exist clearly in the TEM analysis image shown in Figure 8. The filamentous carbons had a diameter of between 10-20 nm, which is believed to be related to the metal particle size [68, 69].

According to the coke deposition data listed in Table 2, when the Ni content is in the range from 5% to 15%, the amount of coke deposition is approximately the same. Further increasing the Ni content to 25 and 35%, the coke deposition declined to a significantly low level (<1wt.%). Based on the work of Sutton et al. [21], for Ni based Al_2O_3 catalysts applied to the biomass gasification process, due the acidic character of the Al_2O_3 support and the easy sintering property of Ni metal, with the increase of Ni content, the amount of coke deposition displayed an increasing trend. However, in this work, with the addition of promoter Zn, the coke deposition appeared as a decreasing trend with the increase of Ni content in the catalysts. This indicated the addition of promoter metal Zn has the advantage of suppressing the coke deposition on the catalyst, which helps increase the thermal stability and lifetime of the catalyst.

For future related work, it is suggested to carry out quantitative analysis to liquid production and also TPO-FTIR analysis to the reacted catalyst to accurately quantify the amount of coke formation on the reacted catalyst. In addition, the optimization of other conditions (e.g. calcination temperature) for catalyst preparation could also be valuable for the design of the

catalyst for hydrogen production from biomass gasification.

4. Conclusions

In this work, NiO-ZnO-Al_2O_3 catalyst with different Ni content and a constant Zn:Al molar ratio of 1:4 prepared by co-precipitation method has been investigated for hydrogen-rich syngas production from the thermochemical conversion of biomass in the form of wood sawdust. It is found that the NiO-ZnO-Al_2O_3 catalysts prepared by co-precipitation method has well-dispersed NiO, $ZnAl_2O_4$ and $NiAl_2O_4$ crystal phases with a particle size of approximate 6-7 nm. Gas production was increased from 49.3 to 74.8 wt.% and the H_2 yield was enhanced from 8.2 to 20.1 mmol g^{-1} wood sawdust with the increase of Ni molar ratio from 5 to 35% when catalysts with different Ni loadings were investigated. The enhanced hydrogen production with the increase of Ni content was suggested to be due to the increased number of catalytic sites (mainly Ni metal based on the XRD and TPR analysis) during the biomass gasification process. While the particle size of metal crystals was not changed significantly with the increase of Ni content due to the promoting effect of ZnO. In addition, with the increase of Ni content and the addition of promoter metal Zn, the coke deposition displayed a decreasing trend. When the Ni content was increased to 25 and 35%, the coke deposition on the used catalyst (<1 wt.%) was negligible.

Acknowledgement

This work was supported by the International Exchange Scheme from the Royal Society (IE110273), UK, and the Faculty of Engineering & IT's Energy and Materials Cluster Scheme and MCR from the University of Sydney.

References

[1] P. Lv, J. Chang, T. Wang, Y. Fu, Y. Chen, J. Zhu, Hydrogen-Rich Gas Production from Biomass Catalytic Gasification, Energy & Fuels, 18 (2003) 228-233.

[2] S. Albertazzi, F. Basile, J. Brandin, J. Einvall, C. Hulteberg, G. Fornasari, V. Rosetti, M. Sanati, F. Trifirò, A. Vaccari, The technical feasibility of biomass gasification for hydrogen production, Catalysis Today, 106 (2005) 297-300.

[3] M.N. Barroso, M.F. Gomez, L.A. Arrúa, M.C. Abello, Hydrogen production by ethanol reforming over NiZnAl catalysts, Applied Catalysis A: General, 304 (2006) 116-123.

[4] C. Wu, P.T. Williams, Ni/CeO_2/ZSM-5 catalysts for the production of hydrogen from the pyrolysis–gasification of polypropylene, International Journal of Hydrogen Energy, 34 (2009) 6242-6252.

[5] M. Inaba, K. Murata, M. Saito, I. Takahara, Hydrogen Production by Gasification of Cellulose over Ni Catalysts Supported on Zeolites, Energy & Fuels, 20 (2006) 432-438.

[6] X. Hao, L. Guo, X. Zhang, Y. Guan, Hydrogen production from catalytic gasification of cellulose in supercritical water, Chemical Engineering Journal, 110 (2005) 57-65.

[7] C. Wu, L. Wang, P.T. Williams, J. Shi, J. Huang, Hydrogen production from biomass gasification with Ni/MCM-41 catalysts: Influence of Ni content, Applied Catalysis B: Environmental, 108–109 (2011) 6-13.

[8] G. Marbán, T. Valdés-Solís, Towards the hydrogen economy?, International Journal of Hydrogen Energy, 32 (2007) 1625-1637.

[9] A.J. Vizcaíno, M. Lindo, A. Carrero, J.A. Calles, Hydrogen production by steam reforming of ethanol using Ni catalysts based on ternary mixed oxides prepared by coprecipitation, International Journal of Hydrogen Energy, 37 (2012) 1985-1992.

[10] X. Deng, J. Sun, S. Yu, J. Xi, W. Zhu, X. Qiu, Steam reforming of ethanol for hydrogen production over NiO/ZnO/ZrO_2 catalysts, International Journal of Hydrogen Energy, 33 (2008) 1008-1013.

[11] R. Muangrat, J.A. Onwudili, P.T. Williams, Influence of alkali catalysts on the production of hydrogen-rich gas from the hydrothermal gasification of food processing waste, Applied Catalysis B: Environmental, 100 (2010) 440-449.

[12] R. Muangrat, J.A. Onwudili, P.T. Williams, Influence of NaOH, Ni/Al_2O_3 and Ni/SiO_2

catalysts on hydrogen production from the subcritical water gasification of model food waste compounds, Applied Catalysis B: Environmental, 100 (2010) 143-156.

[13] K.M.F. Kazi, P. Jollez, E. Chornet, Preimpregnation: an important step for biomass refining processes, Biomass and Bioenergy, 15 (1998) 125-141.

[14] S. Rapagnà, N. Jand, P.U. Foscolo, Catalytic gasification of biomass to produce hydrogen rich gas, International Journal of Hydrogen Energy, 23 (1998) 551-557.

[15] M. Ni, M.K.H. Leung, K. Sumathy, D.Y.C. Leung, Potential of renewable hydrogen production for energy supply in Hong Kong, International Journal of Hydrogen Energy, 31 (2006) 1401-1412.

[16] G. van Rossum, B. Potic, S.R.A. Kersten, W.P.M. van Swaaij, Catalytic gasification of dry and wet biomass, Catalysis Today, 145 (2009) 10-18.

[17] J. Corella, J.M. Toledo, G. Molina, Calculation of the conditions to get less than 2 g tar/m^3 in a fluidized bed biomass gasifier, Fuel Processing Technology, 87 (2006) 841-846.

[18] A. Olivares, M.P. Aznar, M.A. Caballero, J. Gil, E. Francés, J. Corella, Biomass Gasification: Produced Gas Upgrading by In-Bed Use of Dolomite, Industrial & Engineering Chemistry Research, 36 (1997) 5220-5226.

[19] M. Asadullah, S.-i. Ito, K. Kunimori, M. Yamada, K. Tomishige, Biomass Gasification to Hydrogen and Syngas at Low Temperature: Novel Catalytic System Using Fluidized-Bed Reactor, Journal of Catalysis, 208 (2002) 255-259.

[20] W.B. Hauserman, High-yield hydrogen production by catalytic gasification of coal or biomass, International Journal of Hydrogen Energy, 19 (1994) 413-419.

[21] D. Sutton, B. Kelleher, J.R.H. Ross, Review of literature on catalysts for biomass gasification, Fuel Processing Technology, 73 (2001) 155-173.

[22] L. Devi, K.J. Ptasinski, F.J.J.G. Janssen, A review of the primary measures for tar elimination in biomass gasification processes, Biomass and Bioenergy, 24 (2003) 125-140.

[23] K. Tomishige, M. Asadullah, K. Kunimori, Syngas production by biomass gasification using Rh/CeO2/SiO2 catalysts and fluidized bed reactor, Catalysis Today, 89 (2004) 389-403.

[24] J. Nishikawa, T. Miyazawa, K. Nakamura, M. Asadullah, K. Kunimori, K. Tomishige, Promoting effect of Pt addition to Ni/CeO_2/Al_2O_3 catalyst for steam gasification of biomass, Catalysis Communications, 9 (2008) 195-201.

[25] K. Nakamura, T. Miyazawa, T. Sakurai, T. Miyao, S. Naito, N. Begum, K. Kunimori, K.

Tomishige, Promoting effect of MgO addition to Pt/Ni/CeO_2/Al_2O_3 in the steam gasification of biomass, Applied Catalysis B: Environmental, 86 (2009) 36-44.

[26] K. Tomishige, T. Miyazawa, M. Asadullah, S.-i. Ito, K. Kunimori, Syngas productio from gasificatin of biomass over Rh/CeO_2/SiO_2 catalyst: pyrogasification, steam reforming and CO_2 reforming, Journal of the Japan Petroleum Institute, 46 (2003) 322-327.

[27] J. Nishikawa, K. Nakamura, M. Asadullah, T. Miyazawa, K. Kunimori, K. Tomishige, Catalytic performance of Ni/CeO_2/Al_2O_3 modified with noble metals in steam gasification of biomass, Catalysis Today, 131 (2008) 146-155.

[28] M. Zhao, N.H. Florin, A.T. Harris, The influence of supported Ni catalysts on the product gas distribution and H2 yield during cellulose pyrolysis, Applied Catalysis B: Environmental, 92 (2009) 185-193.

[29] P.R. Buchireddy, R.M. Bricka, J. Rodriguez, W. Holmes, Biomass Gasification: Catalytic Removal of Tars over Zeolites and Nickel Supported Zeolites, Energy & Fuels, 24 (2010) 2707-2715.

[30] M. Asadullah, T. Miyazawa, S.-i. Ito, K. Kunimori, K. Tomishige, Catalyst Performance of Rh/CeO2/SiO2 in the Pyrogasification of Biomass, Energy Fuels, 17 (2003) 842-849.

[31] A. Corujo, L. Yermán, B. Arizaga, M. Brusoni, J. Castiglioni, Improved yield parameters in catalytic steam gasification of forestry residue; optimizing biomass feed rate and catalyst type, Biomass and Bioenergy, 34 (2010) 1695-1702.

[32] F. Miccio, B. Piriou, G. Ruoppolo, R. Chirone, Biomass gasification in a catalytic fluidized reactor with beds of different materials, Chemical Engineering Journal, 154 (2009) 369-374.

[33] T. Kimura, T. Miyazawa, J. Nishikawa, S. Kado, K. Okumura, T. Miyao, S. Naito, K. Kunimori, K. Tomishige, Development of Ni catalysts for tar removal by steam gasification of biomass, Applied Catalysis B: Environmental, 68 (2006) 160-170.

[34] K. Tomishige, T. Kimura, J. Nishikawa, T. Miyazawa, K. Kunimori, Promoting effect of the interaction between Ni and CeO_2 on steam gasification of biomass, Catalysis Communications, 8 (2007) 1074-1079.

[35] T. Miyazawa, T. Kimura, J. Nishikawa, S. Kado, K. Kunimori, K. Tomishige, Catalytic performance of supported Ni catalysts in partial oxidation and steam reforming of tar derived from the pyrolysis of wood biomass, Catalysis Today, 115 (2006) 254-262.

[36] H.J. Park, S.H. Park, J.M. Sohn, J. Park, J.-K. Jeon, S.-S. Kim, Y.-K. Park, Steam reforming

of biomass gasification tar using benzene as a model compound over various Ni supported metal oxide catalysts, Bioresource Technology, 101 (2010) S101-S103.

[37] F. Pompeo, N.N. Nichio, O.A. Ferretti, D. Resasco, Study of Ni catalysts on different supports to obtain synthesis gas, International Journal of Hydrogen Energy, 30 (2005) 1399-1405.

[38] P.H. Blanco, C. Wu, J.A. Onwudili, P.T. Williams, Characterization of Tar from the Pyrolysis/Gasification of Refuse Derived Fuel: Influence of Process Parameters and Catalysis, Energy & Fuels, 26 (2012) 2107-2115.

[39] J. Li, B. Xiao, R. Yan, X. Xu, Development of a supported tri-metallic catalyst and evaluation of the catalytic activity in biomass steam gasification, Bioresource Technology, 100 (2009) 5295-5300.

[40] J. Srinakruang, K. Sato, T. Vitidsant, K. Fujimoto, A highly efficient catalyst for tar gasification with steam, Catalysis Communications, 6 (2005) 437-440.

[41] R. Buitrago-Sierra, J. Ruiz-Martínez, J.C. Serrano-Ruiz, F. Rodríguez-Reinoso, A. Sepúlveda-Escribano, Ethanol steam reforming on Ni/Al2O3 catalysts: Effect of the addition of Zn and Pt, Journal of Colloid and Interface Science, 383 (2012) 148-154.

[42] J. Sun, X.-P. Qiu, F. Wu, W.-T. Zhu, from steam reforming of ethanol at low temperature over , and catalysts for fuel-cell application, International Journal of Hydrogen Energy, 30 (2005) 437-445.

[43] A.N. Fatsikostas, D.I. Kondarides, X.E. Verykios, Production of hydrogen for fuel cells by reformation of biomass-derived ethanol, Catalysis Today, 75 (2002) 145-155.

[44] F. Frusteri, S. Freni, V. Chiodo, L. Spadaro, G. Bonura, S. Cavallaro, Potassium improved stability of Ni/MgO in the steam reforming of ethanol for the production of hydrogen for MCFC, Journal of Power Sources, 132 (2004) 139-144.

[45] F. Frusteri, S. Freni, V. Chiodo, L. Spadaro, O. Di Blasi, G. Bonura, S. Cavallaro, Steam reforming of bio-ethanol on alkali-doped Ni/MgO catalysts: hydrogen production for MC fuel cell, Applied Catalysis A: General, 270 (2004) 1-7.

[46] Y. Yang, J. Ma, F. Wu, Production of hydrogen by steam reforming of ethanol over a Ni/ZnO catalyst, International Journal of Hydrogen Energy, 31 (2006) 877-882.

[47] M.-N. Chen, D.-Y. Zhang, L.T. Thompson, Z.-F. Ma, Catalytic properties of Ag promoted ZnO/Al_2O_3 catalysts for hydrogen production by steam reforming of ethanol, International Journal of Hydrogen Energy, 36 (2011) 7516-7522.

[48] J.C. Rodriguez, E. Romeo, J.L.G. Fierro, J. Santamaría, A. Monzón, Deactivation by coking and poisoning of spinel-type Ni catalysts, Catalysis Today, 37 (1997) 255-265.

[49] M. Barroso, M. Gómez, L. Arrúa, M.C. Abello, Steam reforming of ethanol over a NiZnAl catalyst. Influence of pre-reduction treatment with H2, React Kinet Catal Lett, 97 (2009) 27-33.

[50] M. Yang, S. Li, G. Chen, High-temperature steam reforming of methanol over ZnO–Al_2O_3 catalysts, Applied Catalysis B: Environmental, 101 (2011) 409-416.

[51] X. Xiao, X. Meng, D.D. Le, T. Takarada, Two-stage steam gasification of waste biomass in fluidized bed at low temperature: Parametric investigations and performance optimization, Bioresource Technology, 102 (2011) 1975-1981.

[52] W. Wang, Z. Wang, Y. Ding, J. Xi, G. Lu, Partial Oxidation of Ethanol to Hydrogen over Ni–Fe Catalysts, Catalysis Letters, 81 (2002) 63-68.

[53] G. de Souza, V.C. Ávila, N.R. Marcílio, O.W. Perez-Lopez, Synthesis Gas Production by Steam Reforming of Ethanol over M-Ni-Al Hydrotalcite-type Catalysts; M=Mg, Zn, Mo, Co, Procedia Engineering, 42 (2012) 1980-1990.

[54] F. Yan, S.-y. Luo, Z.-q. Hu, B. Xiao, G. Cheng, Hydrogen-rich gas production by steam gasification of char from biomass fast pyrolysis in a fixed-bed reactor: Influence of temperature and steam on hydrogen yield and syngas composition, Bioresource Technology, 101 (2010) 5633-5637.

[55] J. Chen, Y. Qiao, Y. Li, Modification of Ni state to promote the stability of Ni–Al_2O_3 catalyst in methane decomposition to produce hydrogen and carbon nanofibers, Journal of Solid State Chemistry, 191 (2012) 107-113.

[56] G. Li, L. Hu, J.M. Hill, Comparison of reducibility and stability of alumina-supported Ni catalysts prepared by impregnation and co-precipitation, Applied Catalysis A: General, 301 (2006) 16-24.

[57] R. Buitrago-Sierra, J. Ruiz-MartÃnez, J.C. Serrano-Ruiz, F. RodrÃguez-Reinoso, A. SepÃºlveda-Escribano, Ethanol steam reforming on Ni/Al_2O_3 catalysts: Effect of the addition of Zn and Pt, Journal of Colloid and Interface Science, 383 (2012) 148-154.

[58] R. López-Fonseca, C. Jiménez-González, B. de Rivas, J.I. Gutiérrez-Ortiz, Partial oxidation of methane to syngas on bulk $NiAl_2O_4$ catalyst. Comparison with alumina supported nickel, platinum and rhodium catalysts, Applied Catalysis A: General, 437–438 (2012) 53-62.

[59] J. Chen, Y. Qiao, Y. Li, Promoting effects of doping ZnO into coprecipitated Ni-Al_2O_3 catalyst on methane decomposition to hydrogen and carbon nanofibers, Applied Catalysis A: General, 337 (2008) 148-154.

[60] J. Juan-Juan, M.C. Román-Martínez, M.J. Illán-Gómez, Nickel catalyst activation in the carbon dioxide reforming of methane: Effect of pretreatments, Applied Catalysis A: General, 355 (2009) 27-32.

[61] B. Vos, E. Poels, A. Bliek, Impact of Calcination Conditions on the Structure of Alumina-Supported Nickel Particles, Journal of Catalysis, 198 (2001) 77-88.

[62] J. Zhang, H. Xu, X. Jin, Q. Ge, W. Li, Characterizations and activities of the nano-sized Ni/Al_2O_3 and Ni/La–Al_2O_3 catalysts for NH_3 decomposition, Applied Catalysis A: General, 290 (2005) 87-96.

[63] J. Guo, H. Lou, H. Zhao, D. Chai, X. Zheng, Dry reforming of methane over nickel catalysts supported on magnesium aluminate spinels, Applied Catalysis A: General, 273 (2004) 75-82.

[64] J.M. Rynkowski, T. Paryjczak, M. Lenik, On the nature of oxidic nickel phases in NiO/γ-Al_2O_3 catalysts, Applied Catalysis A: General, 106 (1993) 73-82.

[65] A. Ballarini, S. Bocanegra, A. Castro, S. Miguel, O. Scelza, Characterization of $ZnAl_2O_4$ Obtained by Different Methods and Used as Catalytic Support of Pt, Catalysis Letters, 129 (2009) 293-302.

[66] S. Luo, B. Xiao, Z. Hu, S. Liu, X. Guo, M. He, Hydrogen-rich gas from catalytic steam gasification of biomass in a fixed bed reactor: Influence of temperature and steam on gasification performance, International Journal of Hydrogen Energy, 34 (2009) 2191-2194.

[67] M. Zhao, N.H. Florin, A.T. Harris, Mesoporous supported cobalt catalysts for enhanced hydrogen production during cellulose decomposition, Applied Catalysis B: Environmental, 97 (2010) 142-150.

[68] G. Zeng, Q. Liu, R. Gu, L. Zhang, Y. Li, Synergy effect of MgO and ZnO in a Ni/Mg–Zn–Al catalyst during ethanol steam reforming for H2-rich gas production, Catalysis Today, 178 (2011) 206-213.

[69] C.H. Bartholomew, Mechanisms of catalyst deactivation, Applied Catalysis A: General, 212 (2001) 17-60.

Table 1

Theoretical metal composition, particle size and BET surface area of fresh catalysts

Sample	Theoretical Metal Composition (wt.%)[a]			Particle size(nm) (Obtained from XRD data)			BET surface area(m^2 g^{-1})
	Ni	Zn	Al	$ZnAl_2O_4$	$NiAl_2O_4$	NiO	
5NiZn4Al	5.1	21.4	35.4	11	11	-	88.5
10NiZn4Al	10.0	20.0	33.0	11	11	-	89.7
15NiZn4Al	14.7	18.6	30.7	11	11	-	83.2
25NiZn4Al	23.9	16.0	26.3	11	12	12	84.3
35NiZn4Al	32.5	13.4	22.2	11	12	12	95.7

[a] Theoretical metal composition was calculated by the amount of metal divided by the amount of all the metal oxides, like the theoretical Ni composition equals $Ni/(NiO+ZnO+Al_2O_3)$ (wt.%)

Table 2

Mass balance and gas compositions from pyrolysis and steam reforming of wood sawdust in the presence of NiZnAl catalysts with different Ni molar ratios

Catalytic bed	Sand	5NiZnAl	10NiZnAl	15NiZn4Al	25NiZnAl	35NiZnAl
Gas/Wood (wt.%)	33.0	49.3	51.7	60.8	65.6	74.8
Residue/Wood (wt.%)	38.8	37.5	37.5	37.5	37.5	36.3
H_2 Yield (mmol H_2 g^{-1} sample)	2.4	8.2	9.8	11.8	16.9	20.1
Coke deposition (wt.%)	-	2.2	1.7	2.1	0.2	0.1
Gas Composition (Vol.% N_2 free)						
CO	45.5	33.8	32.7	37.3	36.7	36.7
H_2	17.4	34.7	38.1	38.7	46.9	48.1
CO_2	14.5	18.9	19.0	16.2	15.3	15.1
CH_4	14.8	10.2	8.9	6.3	0.9	0.2
C_2-C_4	7.8	2.4	1.3	1.5	0.2	0.0

FIGURE CAPTIONS

Fig. 1. XRD analysis results of the fresh NiZnAl catalysts; (a): 5NiZn4Al; (b): 10NiZn4Al; (c): 15NiZn4Al; (d): 25NiZn4Al; (e): 35NiZn4Al

Fig. 2. SEM results of the fresh NiZnAl catalysts

Fig. 3. TEM results of the fresh NiZnAl catalysts

Fig. 4. TPR results of the fresh NiZnAl catalysts; (a): 5NiZnAl; (b): 10NiZnAl; (c): 15NiZnAl; (d): 25NiZnAl; (e): 35NiZnAl

Fig. 5. GC/MS graphic results from pyrolysis and steam reforming of wood sawdust with sand

Fig. 6. TPO results of the reacted NiZnAl catalysts; (a): reacted 5NiZnAl; (b): reacted 10NiZnAl; (c): reacted 15NiZnAl; (d): reacted 25NiZnAl; (e): reacted 35NiZnAl

Fig. 7. TPO results of the reacted NiO-ZnO-Al_2O_3 catalysts

Fig. 8. TEM results of the reacted NiO-ZnO-Al_2O_3 catalysts with a Ni molar ratio of 15%

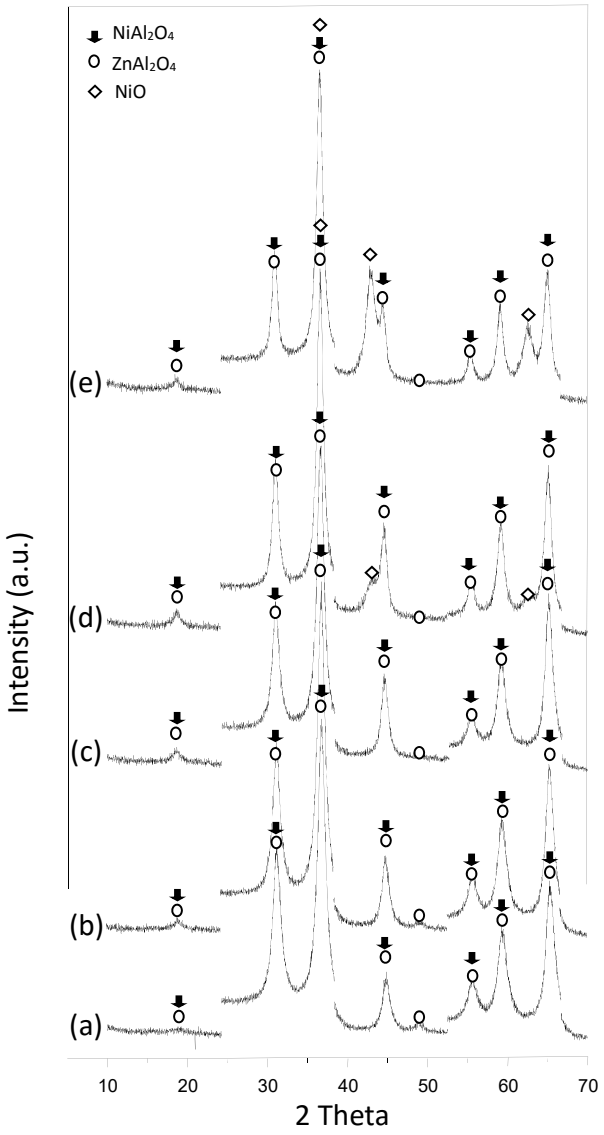

Figure 1 XRD analysis results of the fresh NiZnAl catalysts; (a): 5NiZn4Al; (b): 10NiZn4Al; (c): 15NiZn4Al; (d): 25NiZn4Al; (e): 35NiZn4Al

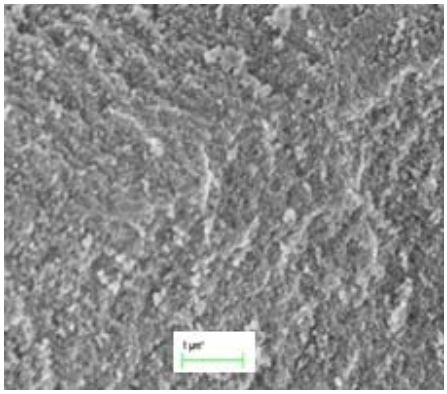

(a) 5NiZnAl catalyst

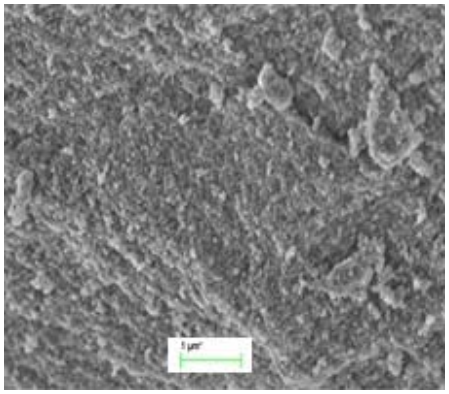

(b) 10NiZnAl catalyst

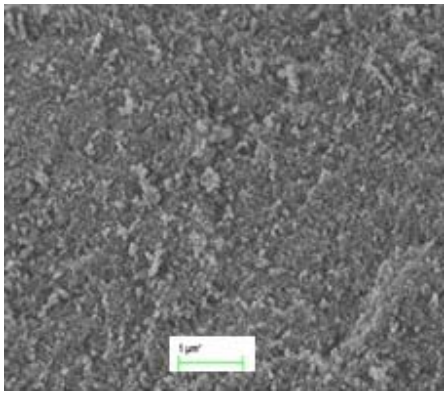

(c) 15NiZnAl catalyst

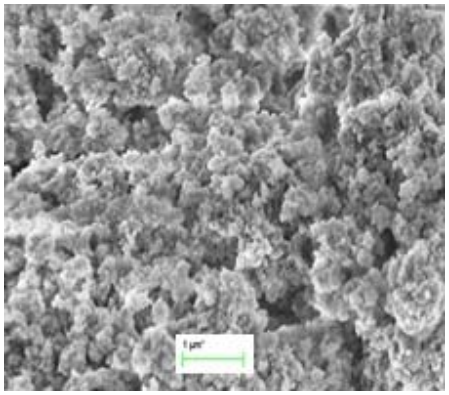

(d) 25NiZnAl catalyst

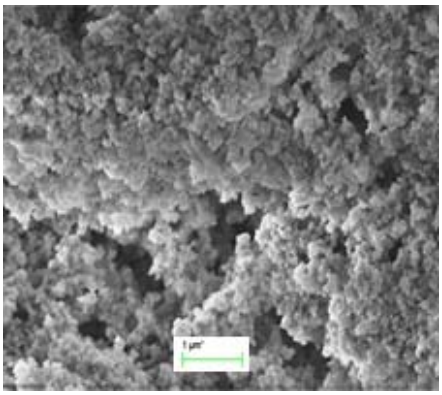

(e) 35NiZnAl catalyst.

Figure 2 SEM results of the fresh NiZnAl catalysts

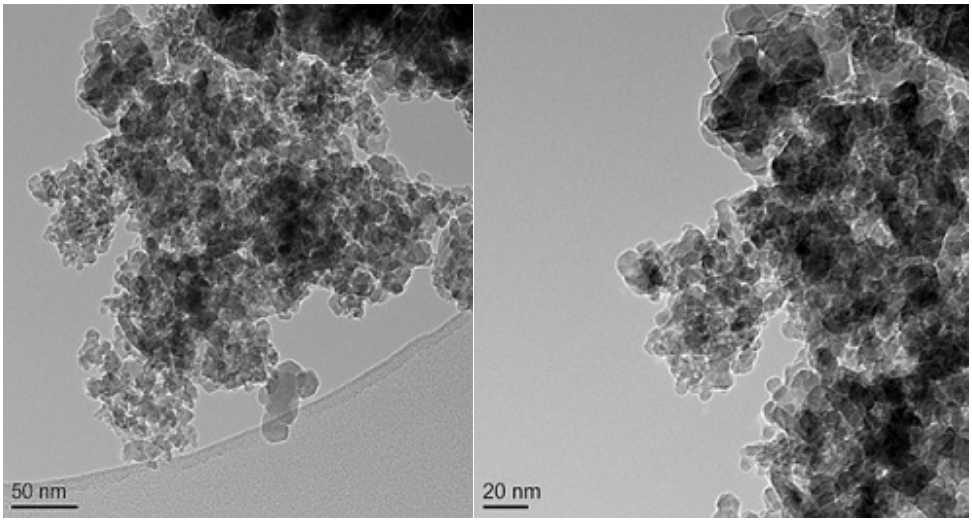

(a): fresh 5NiZn4Al catalyst;

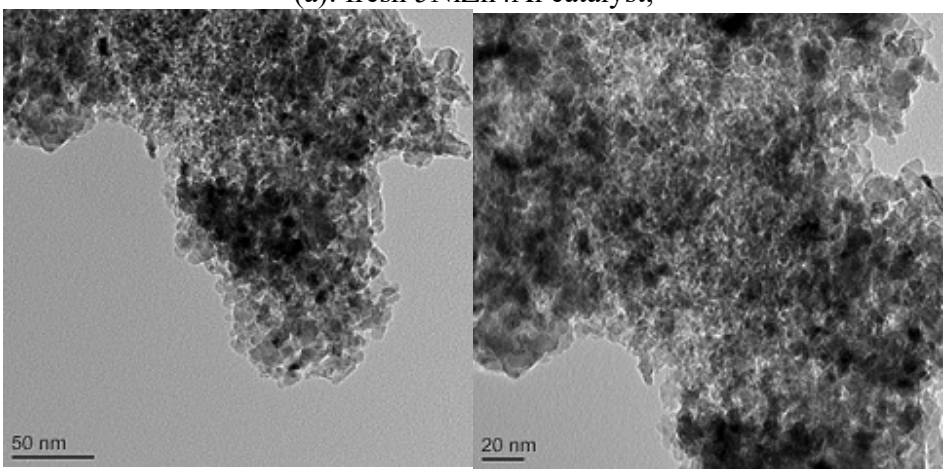

(b): fresh 35NiZn4Al catalyst.

Figure 3 TEM results of the fresh NiZnAl catalysts

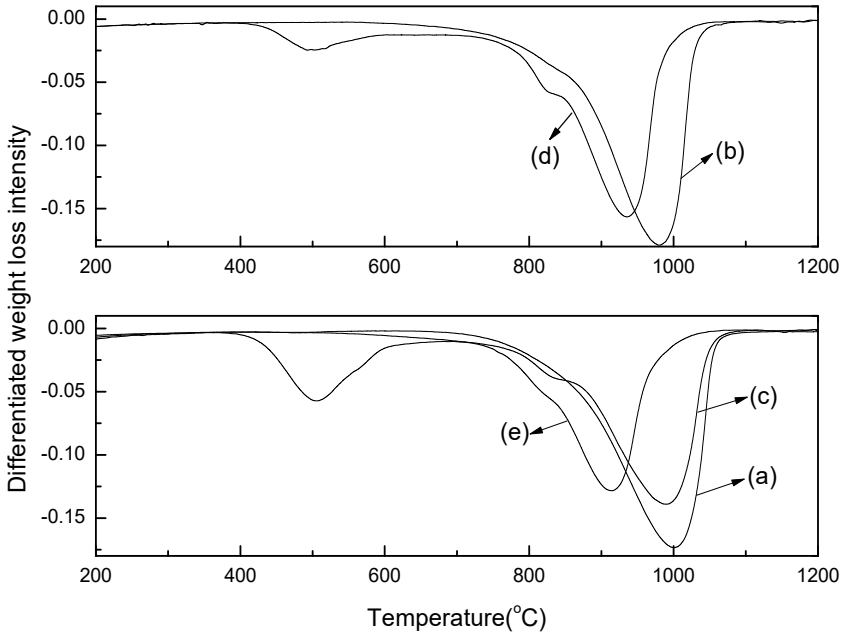

Figure 4 TPR results of the fresh NiZnAl catalysts; (a): 5NiZnAl; (b): 10NiZnAl; (c): 15NiZnAl; (d): 25NiZnAl; (e): 35NiZnAl

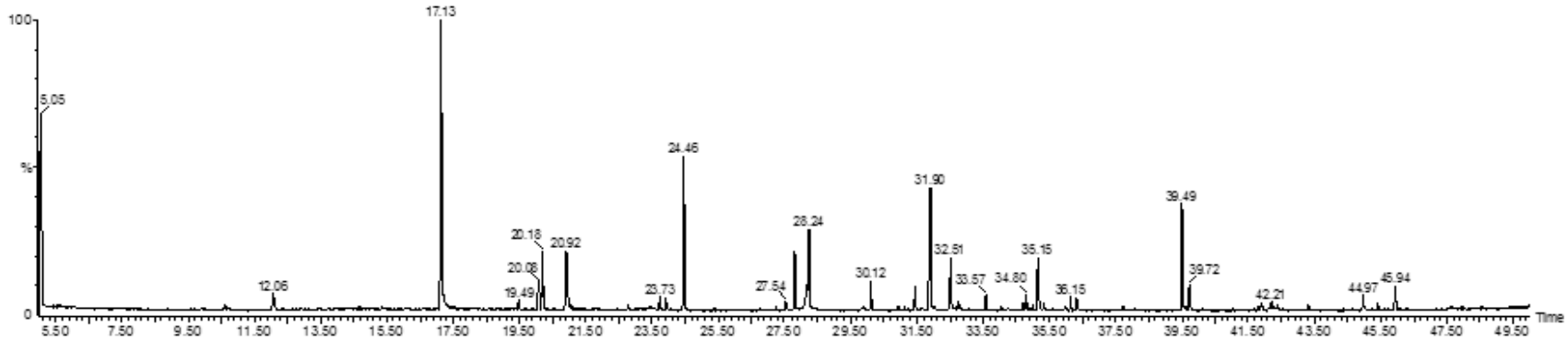

Figure 5 GC/MS graphic results from pyrolysis and steam reforming of wood sawdust with sand

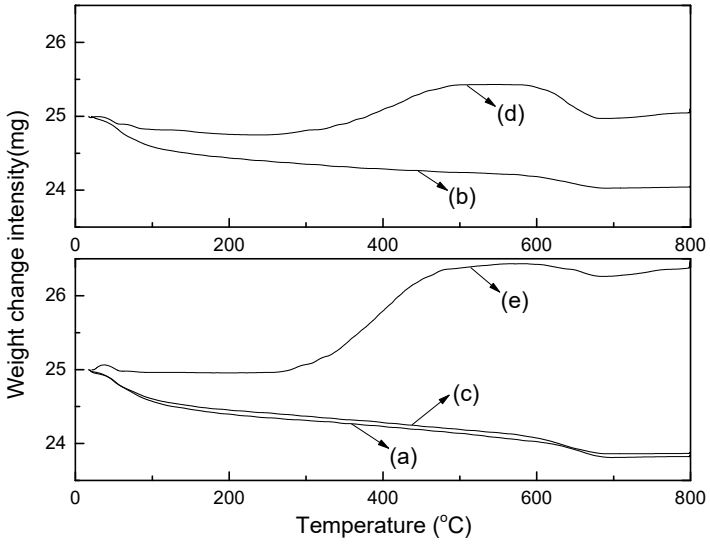

Figure 6 TPO results of the reacted NiZnAl catalysts; (a): reacted 5NiZnAl; (b): reacted 10NiZnAl; (c): reacted 15NiZnAl; (d): reacted 25NiZnAl; (e): reacted 35NiZnAl

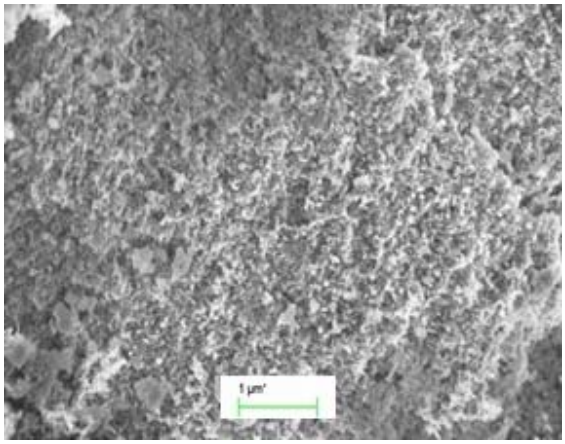

(a) 5NiZnAl

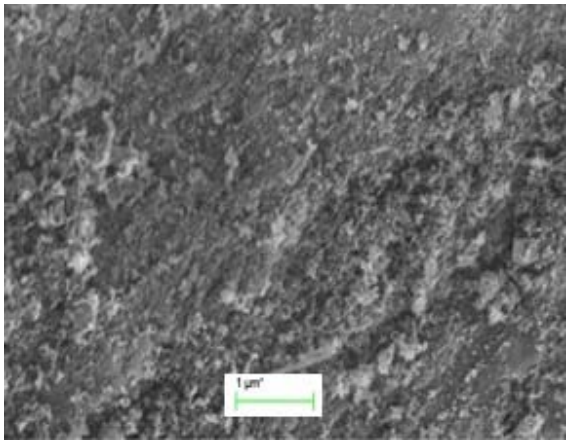

(b) 10NiZnAl

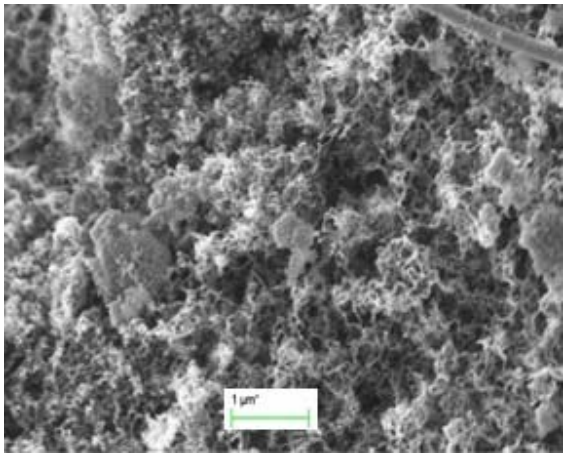

(c) 15NiZnAl

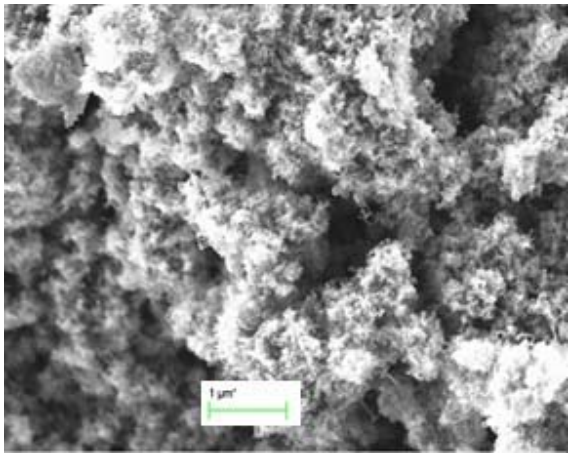

(d) 25NiZnAl

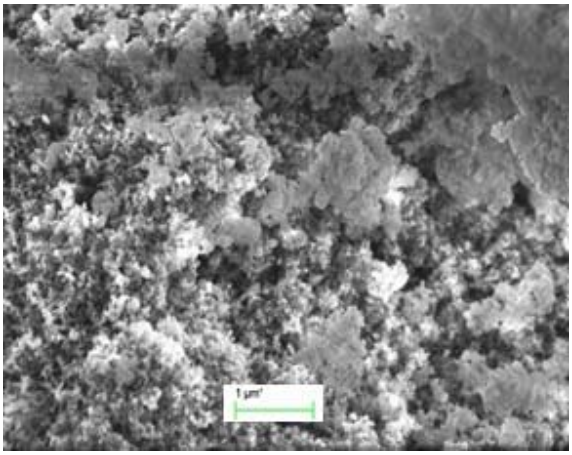

(e): 35NiZn4Al

Figure 7 TPO results of the reacted NiO-ZnO-Al_2O_3 catalysts

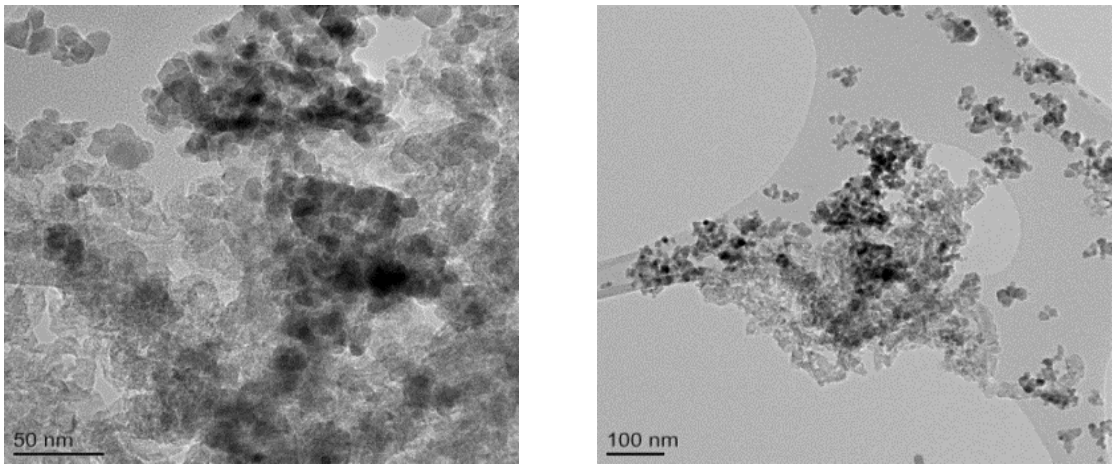

Figure 8: TEM results of the reacted NiO-ZnO-Al_2O_3 catalysts with a Ni molar ratio of 15%